

Modelling of direct metal laser sintering of EOS DM20 bronze using neural networks and genetic algorithms

A. Singh¹, D.E. Cooper², N.J. Blundell³, G.J. Gibbons⁴, D.K. Pratihari⁵

¹ Dept of Mechanical Engineering, IIT Kharagpur, West Bengal, India.

² WMG, University of Warwick, Coventry, CV4 7AL, UK.

³ WMG, University of Warwick, Coventry, CV4 7AL, UK.

⁴ WMG, University of Warwick, Coventry, CV4 7AL, UK.

⁵ Dept of Mechanical Engineering, IIT Kharagpur, West Bengal, India

Abstract: An attempt was made to predict the density and micro-hardness of a component produced by Laser Sintering of EOS DM20 Bronze material for a given set of process parameters. Neural networks were used for process-based-modelling, and results compared with a Taguchi analysis. Samples were produced using a powder-bed type ALM (Additive Layer Manufacturing)-system, with laser power, scan speed and hatch distance as the input parameters, with values equally spaced according to a factorial design of experiments. Optical Microscopy was used to measure cross-sectional porosity of samples; Micro-indentation to measure the corresponding Vickers' hardness. Two different designs of neural networks were used - Counter Propagation (CPNN) and Feed-Forward Back-Propagation (BPNN) and their prediction capabilities were compared. For BPNN network, a Genetic Algorithm (GA) was later applied to enhance the prediction accuracy by altering its topology. Using neural network toolbox in MATLAB, BPNN was trained using 12 training algorithms. The most effective MATLAB training algorithm and the effect of GA-based optimization on the prediction capability of neural networks were both identified.

Keywords: Direct Metal Laser Sintering, Genetic Algorithms, Neural Networks.

1. Introduction

Direct Metal Laser Sintering (DMLS) is an Additive Manufacturing technique, capable of constructing metallic components by depositing and selectively melting successive layers of metal powder [15]. Figure 1 shows the principle of the process, with raw material fed into a processing area by a re-coating mechanism.

In recent years, neural networks have become very useful tool in the modelling of input-output relationships of some complicated systems [1]. They have excellent ability to learn and generalize (interpolate) the complicated relationships between input and output variables. There are different training schemes for these neural networks [2]. Counter Propagation Neural Network (CPNN) and Back Propagation Neural Network

(BPNN) are two designs of neural network, with the approximation efficiency of each varying with the type of data used [11, 16]. Radial basis function network [5] was also used to check and compare the accuracy of modelling, but it did not yield appreciable results. Margaris et al. [3] discussed the implementation of CPNNs. Network optimization concerns the technique used to achieve the optimum number of hidden neurons in a CPNN [4]. BPNNs have been used for a variety of modelling tasks for complex systems [6].

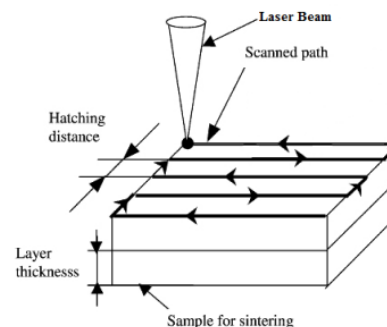


Fig.1. Schematic of DMLS Parameters [8]

The properties of components produced by DMLS depend heavily on fine control of the input parameters, so identifying the precise effect of each parameter is crucial. Wang et al. [7] explored the part shrinkage of samples manufactured by Selective Laser Sintering (SLS), by varying seven process parameters. An experimental design approach was used towards SLS of low carbon steel by Chatterjee et al. [8], where the parameters used were layer thickness and hatching distance, to consider the effects of density, hardness and porosity of sintered components. Ning et al. [9] and Wang et al. [7] used models to intelligently select the parameters for

modelling the DMLS process. One of the notable studies related to the application of soft computing towards laser sintering included the estimation of build time [10]. Comparisons between the applicability of BPNN and CPNN towards manufacturing process (TIG welding) have been demonstrated by Juang et al. [11]. Apart from SLS, multiple designs of neural networks have been used in the past to model different aspects of various other manufacturing processes. Lu et al. [12] worked on modelling the Laser Engineered Net Shaping (LENS) process, where BPNN-based models were applied to control the deposition height of the prototype. For laser welding, Lim and Gweon [13] investigated the application of neural networks in estimating joint strength for pulsed laser spot welding. Balasubramanian et al. [14] discussed about the performance of BPNN for the modelling of stainless steel butt joints.

In this study, a unique comparison of CPNN and BPNN had been carried out in the context of modelling the sample hardness and cross-sectional porosity. To have a better estimation of predictive capability of the two designs, they were trained and tested with three unique data sets. Using MATLAB, several BPNN training algorithms were tested. The effect of a binary-coded GA (Genetic Algorithm) was also studied towards enhancing the predictive capability of a BPNN.

2. Methodology

The following steps were followed to carry out the experiments:-

- Sample production by ALM;
- Metallographic sectioning & polishing;
- Visual examination and hardness tests to obtain the desired output values to be fed into the Neural Network;

The values of the input parameters were Laser Power (kW): 0.75, 1.00, 1.25, 1.50, 1.75; Laser Scan Speed (m/min): 5.0, 6.5, 8.0, 9.5, 11.0; Hatch Distance (mm): 0.25, 0.50, 0.75, and 1.00.

2.1. Techniques used, and developed approaches

After the values for the various experimental runs were obtained, the entire data was assembled in input-output pairs. A total of 99 such pairs were obtained, which were divided into three sets of 89 training values and 10 testing values. These values were then used in the neural network-based modelling task. An artificial neural network (ANN) is a mathematical or computational model that is inspired by the structure and/or functional aspects of biological neural networks. The CPNN is a hybrid network, consisting of an outstar network and competitive filter network. The hidden layer is a Kohonen

network, which categorizes the pattern that was input. The output layer is an outstar array, which reproduces the correct output pattern for the category. The second kind of neural network used in the study was a BPNN, the topology of which is shown in Fig. 2. The numbers of nodes in the input and output layers are N_i and N_o , respectively. The use of a larger number of hidden nodes can potentially improve the accuracy and convergence of the back-propagation (BP) algorithm at the cost of computational processing time [2].

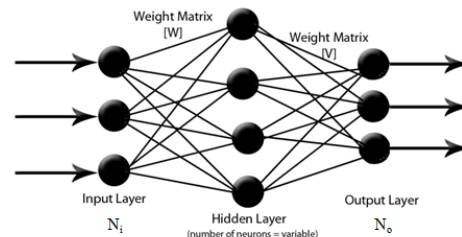


Fig. 2. BPNN Architecture

In the tests carried out, $N_i = 3$ and $N_o = 2$, while the number of neurons in the hidden layer was varied and tested with the help of a Genetic Algorithm (GA). Juang et al. [11], Goh et al. [6] and Margaris et al. [3] discussed the network structures and training schemes in detail. Pratihari [2] discussed the training schemes of BPNN in detail.

A binary-coded GA was used to optimize the topology of the network. Of the two types of errors described above, the GA tends to minimize the training error by choosing the best combination of network parameters, such as number of neurons of the hidden layer 'nh', coefficient of transfer function of the hidden layer 'ah', coefficient of transfer function of the output layer 'ao' (Pratihari [2]). The following steps were used in GA implementation:

- Creation of random population (size of 100). Each chromosome in the population represents a certain combination of 'nh', 'ah' and 'ao';
- Fitness evaluation of each chromosome using the mean square error (MSE) of the BPNN [2], after 10000 iterations, keeping the topology represented by that chromosome into account;
- Tournament-based selection [2] was used to select the pool of better chromosomes;
- Single point crossover and Mutation with respective probabilities of 0.9 and 0.09, forming a new pool of 100 chromosomes and indicating the completion of a generation;
- The process was repeated for 100 generations, and the fittest chromosome was finally chosen;

The modelling was conducted in C++, where codes were written for GA optimized BPNN and CPNN. Using neural network toolbox in MATLAB, analysis of 12 training algorithms was carried out for feed-forward network. C++ coding was performed on a GCC compiler

(version: Dec 20 1999 15:39:08). Minitab v16 was used to perform the Taguchi L9 analysis.

3. Results and discussion

Inputs of the neural network were normalized in the scale of 0 to 1. In neural network toolbox of MATLAB, feed-forward networks were developed using 12 different training algorithms, namely *traingd* (Gradient descent), *traingdm* (Gradient descent with momentum), *traingdx* (Gradient descent momentum with an adaptive learning rate), *trainrp* (Resilient BP algorithm), *traingcf* (Conjugate gradient BP with Fletcher-Reeves updates), *traingcp* (Conjugate gradient BP with Polak-Ribiere updates), *traingcb* (Conjugate gradient BP with Powell-Beale restarts), *traingcg* (Scaled conjugate gradient method), *trainbfg* (BFGS quasi-Newton method), *traingoss* (One step secant method), *trainlm* (Levenberg-Marquardt optimization) and *trainbr* (Levenberg-Marquardt optimization with Bayesian regularization). Three combinations of 89 training and 10 testing cases have hereby been referred to as Set-1, Set-2 & Set-3. The number of neurons in the hidden layer was varied from 2 to 17, keeping the number of unknowns ($5 \times$ number of neurons in the hidden layer) lower than the number of equations (89 training cases). Tests were conducted for 'ah' and 'ao' by individually varying the ranges, and the optimum range was found to be (0.2 to 15.95, in steps of 0.25) and (0.2 to 3.35, in steps of 0.05) for ah and ao, respectively. Table 1 shows the optimum values of the parameters: nh, ah and ao.

The Mean Generalization Error (MGE) represents the mean absolute difference between the normalized values of computed and actual porosity and hardness. The training algorithm shown is the same as the *traingdm* algorithm discussed later in this section in the MATLAB results. For the CPNN, the number of neurons in the competition layer was varied from 2 to 89. The network was allowed to train as long as the MSE was converging towards 0. The loop was terminated the moment the MSE started diverging. Upon analysing the final MSE before divergence occurred, the best network topology was chosen.

Upon increasing the number of hidden neurons, up to a certain number the pattern was uniform. After that, there were indications of improper (over/under)-training. For all the three cases, the best values for MGE were obtained between 25 to 30 neurons. The BPNN took 10000 iterations (for NN weight modification) converge to the specified MGE, while the CPNN took only 4 iterations. Table 2 shows the best CPNN configuration (lowest MSE-based analysis).

Table 1. BPNN Results

Set	Optimum Parameters			MGE
	n_h	a_h	a_o	
Set-1	15	8.75	2.10	0.1076
Set-2	15	8.50	2.25	0.1300
Set-3	16	8.75	2.10	0.1676

Table 2. CPNN Results

Set	No. hidden neurons	MGE
Set-1	30	0.1110
Set-2	28	0.1393
Set-3	29	0.1320

Table 3. MATLAB Results

Algorithm	Set-1	Set-2	Set-3
<i>traingd</i>	0.1334 (17)	0.1304 (14)	0.1798 (8)
<i>traingdm</i>	0.1442 (16)	0.1336 (12)	0.1392 (5)
<i>traingdx</i>	0.1006 (10)	0.1387 (11)	0.1024 (16)
<i>trainrp</i>	0.0843 (10)	0.1255 (13)	0.1920 (10)
<i>traingcf</i>	0.0896 (10)	0.1066 (13)	0.1605 (9)
<i>traingcp</i>	0.1016 (17)	0.1404 (14)	0.1636 (13)
<i>traingcb</i>	0.1473 (16)	0.1170 (12)	0.1845 (14)
<i>traingcg</i>	0.1044 (11)	0.1329 (13)	0.1539 (11)
<i>trainbfg</i>	0.1056 (16)	0.1357 (14)	0.1577 (15)
<i>traingoss</i>	0.1249 (16)	0.1238 (14)	0.0964 (14)
<i>trainlm</i>	0.1298 (13)	0.1457 (7)	0.1659 (12)
<i>trainbr</i>	0.0990 (9)	0.1399 (14)	0.1594 (13)

Feed-forward back-propagation neural network was trained using 12 different training algorithms; the results have been compared in this section. As training parameters, the number of iterations/epochs was set to a maximum of 10000. The performance goal, based on the MSE, was set to 0 (zero) and rest all other training parameters were at their default values. For all the networks, the one hidden layer with a *tansig* activation function and one output layer with *purelin* activation function were used. The value of 'nh' was varied from 2 to 17. The best approximation was identified as the network topology (i.e., the number of neuron in the hidden layer) with the least MSE at the completion of the training process. Table 3 displays the values of MGE for various training algorithms. The number of neurons of the hidden layer for the same network has been indicated in the bracket. The MATLAB training algorithm named

trainidx turned out to be the most accurate one with an average MGE of 0.1139 on the normalized scale.

Using the Taguchi L9 analysis, laser scan speed was found to have the maximum effect on both the outputs, while laser power and hatch distance were found to have the minimum effect on porosity and mean hardness, respectively. Figure 3 overleaf, compares the predicted values of the two outputs with their respective actual values for the test cases (using trainrp for Set-1)

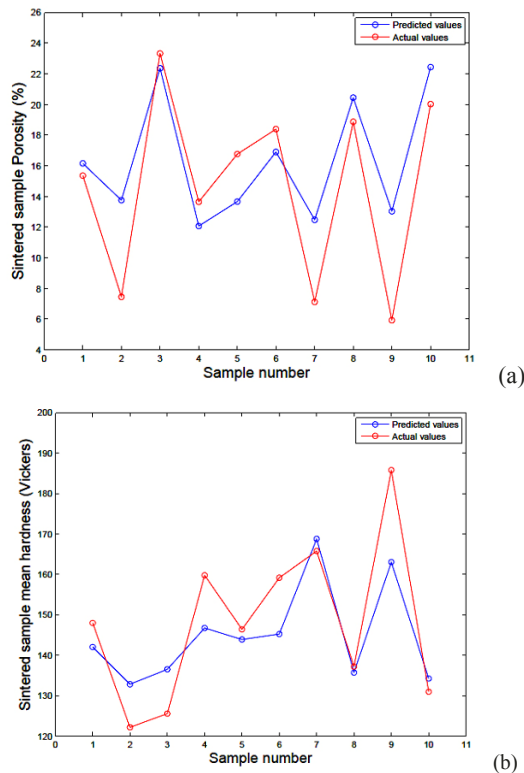


Fig. 3. Actual vs. Predicted values of (a) porosity and (b) mean hardness for the test cases

4. Conclusion

The MATLAB training algorithm “trainidx” was found to be the most accurate, with an average Mean Generalisation Error (MGE) of 0.1139 on a normalized (0 to 1) scale. Counter Propagation and Genetic Algorithm (GA) optimized-Back Propagation Neural Networks (BPNN) had average MGE values of 0.1274 and 0.1350, respectively. The training time for CPNN was much shorter than for BPNN. Laser Scan Speed was seen to have the greatest influence on both the outputs, using the Taguchi method. The use of GA-based optimization successfully reduced the MGE for BPNN trained by the gradient descent with momentum algorithm from 0.1350 to 0.1274.

References

- [1] Freeman JA, Skapura DM, (1991) Neural Networks: Algorithms, Application and Programming Techniques, Addison-Wesley,
- [2] Pratihari DK, (2008) Soft Computing, Narosa Publishing House, New Delhi.
- [3] Margaris A, Souravlas S, Kotsialos E, Roumeliotis M, (2007) Design and Implementation of Parallel Counterpropagation Networks Using MP, Informatica, 18:79-102
- [4] Dong Y, Sun C, Tai X, (2007) An Adaptive Counter Propagation Network, Eighth ACIS International Conference on Software Engineering, Artificial Intelligence, Networking, and Parallel/Distributed Computing (IEEE Transactions), Qingdao, 695 – 700
- [5] Park JS, Sandberg IW, (1991) Universal Approximation using Radial-Basis-Function Networks, Neural Computation 3 (MIT Press), 246-257
- [6] Goh ATC, (1995) Back-propagation neural networks for modelling complex systems, Artificial Intelligence in Engineering 9, 143-151
- [7] Wang RJ, Wang L, Zhao L, Liu Z, (2007) Influence of process parameters on part shrinkage in SLS, International Journal of Advanced Manufacturing Technology 33:498 – 504
- [8] Chatterjee AN, Kumar S, Saha P, Mishra K, Roy Choudhury A, (2003) An Experimental design approach to selective laser sintering of low carbon steel, JMPT 136:151 – 157
- [9] Ning Y, Fuh JYH, Wong YS, Loh HT, (2004) An Intelligent parameter selection system for the direct metal laser sintering process, International Journal of Production Research 42:183 – 199
- [10] Mungunia J, Ciurana J, Riba C, (2009) Neural-network-based model for build-time estimation in selective laser sintering, Proceedings of the Institution of Mechanical Engineers, Part B: Journal of Engineering Manufacture, 995 – 1002
- [11] Juang SC, Tarnq YS, Lii HR, (1998) A comparison between the back-propagation and counter-propagation networks in the modelling of the TIG welding process, JMPT 75:54 – 62
- [12] Lu ZL, Li DC, Lu BH, Zhang AF, Zhu GX, Pi G, (2010) The prediction of the building precision in the Laser Engineered Net Shaping process using advanced network, Optics and Lasers in Engineering 48:519-525
- [13] Lim DC, Gweon DG, (1999) In-Process Joint Strength Estimation in Pulsed Laser Spot Welding Using Artificial Neural Networks, Journal of Manufacturing Processes 1:31 – 42
- [14] Balasubramanian KR, Buvanashakaran G, Sankaranarayanan K, (2010) Modelling of laser beam welding of stainless steel sheet butt joint using neural networks, CIRP Journal of Manufacturing Science and Technology 3:80 – 84
- [15] Das S, Wohlert W, Beaman JJ, Bourell DL, (1998) Producing Metal Parts with Selective Laser Sintering/Hot Isostatic Pressing, JOM 50 (12):17 – 20
- [16] Dharia A, Adeli H, (2003) Neural Network model for rapid forecasting of freeway link travel time, Engineering Applications of Artificial Intelligence 16:607 – 613.

A thermo-mechanical model for laser processing of metallic alloys

A. Suárez, J. M. Amado, M. J. Tobar, A. Yáñez
Universidade da Coruña, D. de Ingeniería Industrial II, Ferrol, E-15403, Spain.

Abstract. Among the wide scope of laser materials processing techniques stand the use of high power laser as an alternative tool in standard manufacturing process as cutting, welding or bending and forming. The nature of the laser beam energy profile provides with a controlled and precise heat input in the material minimizing mechanical and microstructure distortions. The development of analytical or numerical models is useful not only to get an insightful understanding of the underlying aspects but also to optimize process parameters and reduce experimental trials. Then numerical methods are often preferred over the analytical ones as they allow accommodating for variations in the process such as geometry or temperature dependent material properties. A 3D customized transient FEM model was developed to understand the main features of the metallurgical and thermo-mechanical phenomena and make accurate predictions. The metallurgical model is based on the carbon diffusion during the austenitization process through 1D diffusion models. Martensitic transformation and backtempering are included. Experimental tests for the validation of the model are also discussed.

Keywords: thermomechanical, metallurgical, phase transformations, laser cladding

1. Introduction

The laser cladding technique allows the deposition of low dilution tracks of molten material on a metal substrate, a metallurgical bond between fed material and the substrate is achieved during solidification.

One of the main concerns is the development of high residual stresses. They affect the working life of the part due to the enhancement of the susceptibility to both fatigue and stress-corrosion. Additionally workpiece will show distortion and cracks.

Experimental methods to measure residual stresses are usually complex. In contrast, computer simulations can produce an insightful understanding of the underlying aspects of the process.

Both 2D and 3D CFD models of the laser cladding have been studied [1-3], but they are not easily coupled with mechanical analysis; so heat conduction models are preferred. The effect of deposition patterns on deflection of the workpiece [4], the cladding track geometry was also evaluated inside simple plasticity models [5-7].

Phase transformations were studied mainly for laser hardening. Several authors [8,9] based their work on the simple kinetic model [10], others use data from TTT/CCT diagrams and the Johnson-Mehl-Avrami (JMA) equation [11]. Also exist 2D kinetic models coupled to 3D FEM models [12], but 1D kinetic models are faster [13]. Backtempering due to adjacent laser passings was also studied [14] inside a tempering model based on the JMA equation.

Metallurgy received less attention in laser cladding. In [15] 3D models using the software SYSWELD are developed including metallurgical transformations and coupled with the mechanical analysis.

In this paper a metallurgical model based on 1D carbon diffusion for steels was developed. It includes the tempering due to the deposition of the contiguous cladding tracks in a JMA approach. This model was coupled with a previously developed thermomechanical model [16] already published.

2. Model description

In the model [16] thermal and mechanical fields are sequentially coupled. The simulation starts with a transient thermal analysis. These results are applied as thermal load for the subsequent quasistatic mechanical analysis. Birth & Death techniques are used for the simulation of the material deposition.

Metallurgy is fully coupled with both thermal and mechanical analysis. Each thermal load step is solved starting by a pure thermal step and the subsequent metallurgical step, allowing the change of material properties during the analysis. The phase volume fractions are stored, so during each mechanical step the properties of any element can be calculated. Each element has assigned a vector with all required information. It is implemented as a main routine that controls the transition between stability regions of different phases, according to the element temperature. Specific routines containing the kinetic models are called to compute the phase evolution.

Initially the steel sample is in a ferritic-pearlitic microstructure. The carbon content of pearlite (0.8%) is much higher than in ferrite, so above austenitization temperature, austenite grains nucleate in pearlite. Ferrite will transform at higher temperatures. During the transformation the lattice changes from BCC to FCC, increasing density around 4%.

Austenitization is regarded as a two-step process [8]. The first stage is the fast intragranular carbon diffusion in pearlite. The second step is the intergranular diffusion, homogenizing the carbon distribution [2]. Each of these two steps is simulated in a different 1D diffusion model.

The first model uses the pearlite interlamellar spacing to calculate cementite and ferrite lamellae widths (Fig. 1) from the carbon concentration of these phases. The intragranular diffusion distance is divided in intervals and carbon concentration is calculated in each of them. Complete austenitization is achieved when carbon concentration reaches 90% of its value in pearlite.

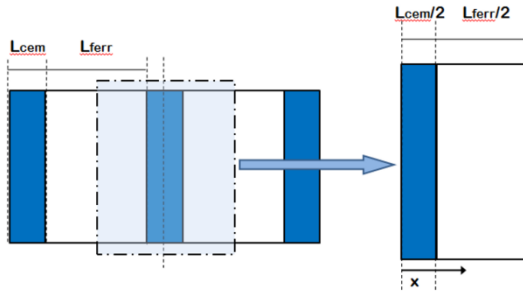


Fig. 1. Schematic view of the geometrical model for the pearlite dissolution.

The second model uses the pearlite grain size and the carbon content to calculate the diffusion distance between grains. This distance is divided in intervals, considered austenitized when carbon content is above austenite critical value. The fraction of austenitized intervals gives the austenite percentage. In between temperatures A_{C1} and A_{C3} the maximum percentage is adjusted using the C-Fe phase diagram.

Both models are based on the carbon diffusion from a homogeneous phase of width h and initially constant carbon content C_0 , from which carbon diffuses to a region of lower carbon content (Fig. 1).

The 1D diffusion equation is applied [8]:

$$\frac{dC(x,t)}{dt} = D(T) \frac{\partial C(x,t)}{\partial x} \quad (1)$$

With the previous initial condition, considering symmetry at the origin and one reflection at the end of the cell ($x=LT$), the following equation results:

$$C(x,t) = \frac{C_0}{2} \left[\operatorname{erf} \left(\frac{(h-x)}{2\sqrt{D(T)t}} \right) + \operatorname{erf} \left(\frac{(h+x)}{2\sqrt{D(T)t}} \right) + \operatorname{erf} \left(\frac{(h-(2LT-x))}{2\sqrt{D(T)t}} \right) + \operatorname{erf} \left(\frac{(h+(2LT-x))}{2\sqrt{D(T)t}} \right) \right] \quad (2)$$

The temperature dependent diffusion coefficient is calculated as follows:

$$D(T) = D_0 \exp \left(-\frac{Q}{RT} \right) \quad (3)$$

Where D_0 is the diffusion coefficient, Q is the activation energy of carbon diffusion, R is Boltzmann's constant and T is the absolute temperature. The carbon diffusion from austenite to ferrite at an isothermal temperature and different times is represented in Fig. 1.

The main cooling mechanism is the heat conduction to the workpiece in a "self-quenching" process, producing martensite. The crystalline structure changes from FCC to BCT by means of a displacive transformation without diffusion depending only on the degree of sub cooling below the martensite start temperature (M_s). It is modeled using the Koistinen-Marburger equation:

$$f_M = 1 - \exp(-\alpha(M_s - T)) \quad (4)$$

Where α is a constant dependent on the transformation rate and the steel composition. Usually, for steels with carbon content smaller than 1.1 % $\alpha = 0.011$ [24].

The previously formed martensite undergoes a heating process during the next laser passing causing its tempering: decomposing of martensite into a stable microstructure of ferrite with dispersed carbides.

Tempering starts at 100°C and continues up to A_{C1} temperature. Between 100°C and 200°C a finely dispersion of ϵ carbide and transition metal carbides are formed [18]. At temperatures between 200°C and 300°C takes place the transformation of retained austenite into ferrite and cementite. At higher temperatures only cementite is formed and the carbides coarsen, softening the microstructure [18].

The process is simulated with the using the JMA equation. Parameters were taken from Lakhkar et al. [14]

$$f_{TM} = f_M \left(1 - \exp(1-kt)^n \right) \quad (5)$$

where,

$$k = k_0 \exp \left(-\frac{Q}{RT} \right) \quad (6)$$

Being f_M the maximum fraction of martensite, Q the activation energy and n and k_0 experimentally derived constants. The equation is valid for isothermal conditions, so the laser process is subdivided into a series of

isothermal steps (Fig. 2), and the effect of each step is added according to the Scheil's additive rule [17]. Hardness is commonly calculated by means of the rule of mixtures [17]: a linear combination of the hardness of each phase, weighted by its volume fraction.

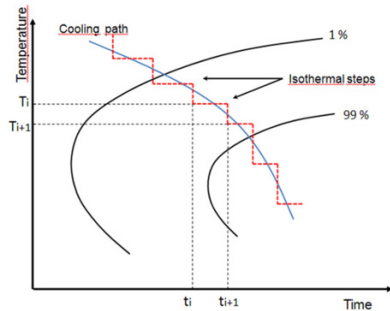


Fig. 2. Discretization of the cooling process into a series of isothermal steps.

3. Experimental

Laser surface melting tests were performed to validate the metallurgical model using carbon steel plates of AISI 1045 and a 2 kW CO₂ laser. The tests consisted of 3 laser tracks of 80 mm length on plates of 100x50x10 mm with velocity of 5 mm/s, 1200W of laser power and a 4 mm laser spot (TEM01*). Different distances between tracks were tested to study martensite tempering.

Laser cladding tests with single and multiple cladding tracks were performed using a 2.2 kW Nd:YAG laser with a coaxial laser cladding nozzle. 80 mm length tracks were deposited on plates as before with parameters: 1800 W of power, a speed of 5 mm/s and a powder flow rate of 0.48 g/s. The samples were cut, mechanically grounded, polished and etched with Nital 3 to reveal the microstructure. Microhardness was also measured.

4. Results

The FEM mesh contains hexahedral elements in the zone below the laser scans and coarse tetrahedral elements in the rest of the plate (126590 elements and 89468 nodes).

Results for 2 and 4 mm spacing are shown in Fig. 3. Absorptivity of the plate was tuned using these results. The calculated melted zones, heat affected zones (HAZ) and tempered zones are similar to the experimental ones. Hardness profiles are in good agreement with maximum errors of about 16% and typical errors below 6%. The maximum differences between the width and depth of the calculated HAZ are about 300 μm . The effect of tempering is especially important for 2 mm spacing tests, but also noticeable for the 4 mm ones. The melted zones obtained are connected when the spacing is 2 mm. The simulated melted zones are in good agreement except for

the last track of this sample: 40% underestimated in depth, due to the neglecting of Marangoni convection.

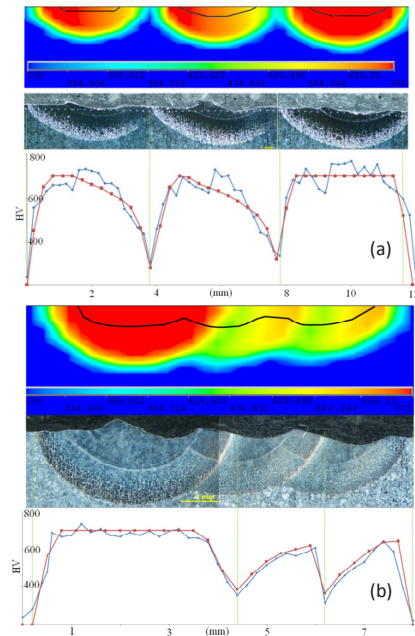


Fig. 3. Results of the laser surface melting tests, spacing between laser passings: (a) 4 mm (first track at left); (b) 2 mm (first track at right).

Four cladding tracks of AISI H13 tool steel on plates of the same steel were simulated with a mesh composed of 57329 elements and 48176 nodes. Each cladding track deposited cools very fast by heat conduction to the steel plate, producing martensite. During the deposition of the contiguous cladding track reheating produces the tempering of the generated martensite so at the end of the simulation only the last track is fully martensite (Fig. 4). The final hardness map is shown in Fig. 5 (a).

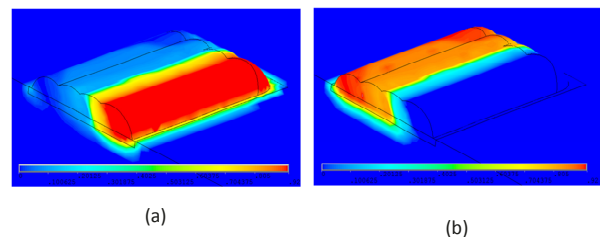


Fig. 4. Phase volume fractions calculated with the laser cladding model (after final cooling): (a) martensite; (b) tempered martensite.

Martensitic transformation has an important impact on the stresses. During the heating the contraction caused by the transformation counteracts the thermal expansion, and the opposite happens during cooling down. Thus the strains are lower than without phase transformation. However this is not true for stresses: the higher yield strength of martensite could lead to higher stresses.

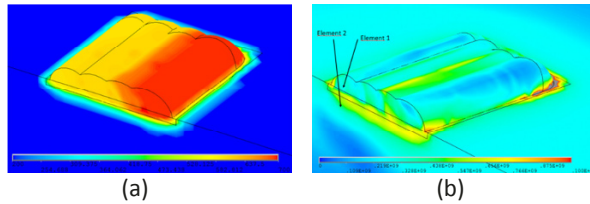


Fig. 5. (a) Final hardness profile and (b) Von Mises equivalent stress calculated with the laser cladding model.

Von Mises equivalent stress is represented in Fig. 5(b). The last clad track has a high percentage of martensite and shows low compressive stresses. The highest stresses are located in the interfaces between the tracks and the plate. The Von Mises stress history of 2 elements is shown in Fig. 6. The elements are situated in: 1) clad track; 2) plate (untransformed zone). The temperature history of 1 is also represented. Element 2 shows a typical profile without phase transformations, during the multitrack deposition process: valleys when the material is hot and peaks when it is cold. Element 1 suffers complete martensitic transformation, generating a stress reversal from tensile to compression during the cooling, producing two peaks instead of one and final stresses lower than before.

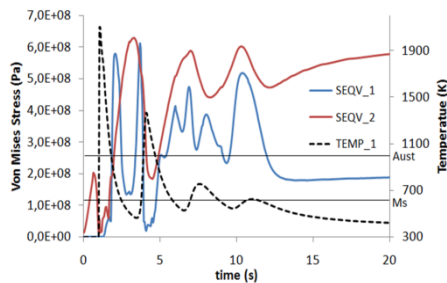


Fig. 6. Von Mises stress and temperature histories calculated for two elements from the laser cladding model.

5. Conclusions

A 3D FEM model was developed for the thermomechanical and metallurgical simulation of laser hardening and laser cladding techniques. The metallurgical model simulates some of the phase transformations in steels: austenitization, martensite transformation and tempering. 1D carbon diffusion models were used for the simulation of the two steps of the austenitization process and tempering. Metallurgy was coupled with the thermomechanical simulations to compute the strains and stresses. Martensite has a great influence on the final stress profile, as it was expected. Experimental tests of laser surface melting show good agreement with the calculated melted zones, HAZ and hardness values

References

- [1] A.F.A. Hoadley and M. Rappaz. A thermal model of laser cladding by powder injection. *Metall. Trans. B*, 23:631-642, 1992.
- [2] M. Picasso, C.F. Marsden, J.D. Wagniere, A. Frenk, and M. Rappaz. A simple but realistic model for laser cladding. *Metallurgical and materials transactions B*, 25:281-291, 1994.
- [3] J. Choi, L. Han, and Y. Hua. Modeling and experiments of laser cladding with droplet injection. *J. Heat Transfer*, 127:978-987, 2005.
- [4] A.H. Nickel, D.M. Barnett, and F.B. Prinz. Thermal stresses and deposition patterns in layered manufacturing. *Materials Science and Engineering*, 317:59-64, 2001.
- [5] R. Jendrzejewski, G. Sliwinski, M. Krawczuk, and W. Ostachowicz. Temperature and stress during laser cladding of double-layer coatings. *Surface and Coatings Technology*, 201:3328-3334, 2006.
- [6] A.M. Deus. A thermal and mechanical model of laser cladding. PhD thesis, Urbana, Illinois, 2004.
- [7] M.J. Tobar, A. Suárez, J.C. Álvarez, J. M. Amado, and A. Yáñez. A 3D transient FEM analysis of residual stress generation during laser cladding. *Proceedings of the LANE 2007*.
- [8] M. Davis, P. Kapadia, J. Dowden, W.M. Steen and C.H.G. Courtney. Heat Hardening of Metal Surfaces with a Scanning Laser Beam. *Journal of Physics D: Applied Physics* 19 (1986).
- [9] R. Patwa and Y.C. Shin. Predictive modeling of laser hardening of AISI 5150H steels. *International Journal of Machine Tools and Manufacture* 47 (2007).
- [10] M.F. Ashby and K.E. Easterling. Transformation hardening of steel surfaces by laser beams-I Hypo-eutectoid steels. *Acta Metallurgica*, 32:1935-1948, 1984.
- [11] M.J. Tobar, C. Álvarez, J.M. Amado, A. Ramil, E. Saavedra and A. Yáñez. Laser transformation hardening of a tool steel: simulation based parameter optimization and experimental results. *Surface and Coatings Technology*, 200:6362-6367, 2006.
- [12] S. Skavarenina and Y.C. Shin. Predictive modeling and experimental results for laser hardening of AISI 1536 steel with complex geometric features by a high power diode laser. *Surface and Coatings Technology*, 201:2256-2269, 2006.
- [13] G.N. Haidemenopoulos. Coupled thermodynamic/kinetic analysis of diffusional transformations during laser hardening and laser welding. *Journal of Alloys and Compounds*, 320:302-307, 2001.
- [14] R.S. Lakhar, Y.C. Shin, and M.J.M. Krane. Predictive modeling of multi-track laser hardening of AISI 4140 steel. *Materials Science and Engineering A*, 253:501-5028, 2008.
- [15] F. Brückner, D. Lepski, and E. Beyer. Calculation of stresses in two and three dimensional structures generated by induction assisted laser cladding. Munich: *Proceedings of the Fifth International WLT-Conference Lasers in Manufacturing, LiM 2009*.
- [16] A. Suárez, J.M. Amado, M.J. Tobar, A. Yáñez, E. Fraga, and M.J. Peel. Study of residual stresses generated inside laser cladded plates using FEM and diffraction of synchrotron radiation. *Surface and Coatings Technology* 204 (2010).
- [17] H. Mehrer. *Diffusion in Solids Fundamentals, Methods, Materials, Diffusion-Controlled Processes*. Springer, 2007.
- [18] G. Roberts, G. Krauss and R. Kennedy. *Tool Steels*. ASM International, 2009.

Transient numerical simulation of CO₂ laser fusion cutting of metal sheets: Simulation model and process dynamics

Stefanie Kohl^{1,2}, Karl-Heinz Leitz^{1,2} and Michael Schmidt^{1,2}

¹ University of Erlangen-Nürnberg, Chair of Photonic Technologies, Paul-Gordan-Str. 3, D-91052 Erlangen, Germany

² Erlangen Graduate School in Advanced Optical Technologies, Paul-Gordan-Str. 6, D-91052 Erlangen, Germany

Abstract. Simulations are a versatile tool of increasing importance for profound analysis and comprehensive understanding of laser-based material processing. Based on our simulation model of laser-matter interaction, we developed a numerical three-dimensional model for the transient simulation of fusion cutting of sheet metal. This model is based on the finite-volume method (FVM) and covers various laser-metal interaction mechanisms, such as multiple surface reflection and absorption according to Fresnel, but also more complex interactions like absorption in the metal plasma. In this study, we focused on a Gaussian shaped CO₂ laser beam applied for the cutting and steel sheets. The implemented physics include fluid and vapor dynamics according to Navier-Stokes, heat conduction, the surface tension of the liquid-vapor interface and the modeling of the enthalpies of fusion and vaporization. As accurate input parameters are crucial for any simulation, special focus was put on the implementation of material properties at temperatures around the melting point. The additional modeling of inert process gas ensures realistic blow-out of the molten material. Furthermore, adaptive meshing enables high calculation accuracy in the areas of interest while minimizing computation time drastically.

Keywords: Laser Fusion Cutting, Laser Cutting Simulation; Finite Volume Method

1. Introduction

Laser material processing attains more and more importance in production technology. Since laser cutting represents a contact and force-free as well as a precise and highly flexible cutting tool, it is the most widespread representative among all these technologies. Though laser cutting does not have to face such severe process errors like pores and humping which complicate laser welding, its simulation is still of major importance both from a scientific as well as an industrial point of view. Since simulations enable the variation of basically all the process and material parameters as well as they offer virtually unlimited accessibility of the work piece and its properties during the process, they are an indispensable tool for both examination and planning of the cutting process.

Many of the existing models available for laser cutting only focus on certain aspects of the process or disregard certain interactions. The model presented in this paper, however, aims at covering the different mechanisms and interactions of laser cutting comprehensively, facilitating high-accuracy modeling of the process based on its underlying physical equations.

2. Simulation model

All modeling was done using the open source computational fluid dynamics (CFD) software package OpenFOAM® (Open Field Operation and Manipulation), which has proved to be a suitable environment for the simulation of a multitude of laser material interaction processes for many years [1-2]. It represents a toolbox of modules for the simulation of complex numerical problems based on partial differential equations, such as fluid flows, heat transfer, solid dynamics as well as electromagnetics. Its open and modular structure enables the flexible implementation of the different interaction mechanisms between laser and material as well as subsequent processes like heat conduction, melt and vapor dynamics and phase transitions.

All liquid-vapor surfaces within the model are regarded as free surfaces and as such they were reconstructed based on their volume fraction making use of a volume-of-fluid (VOF) approach [3]. The size of the time steps is adapted dynamically and derived from the Courant number [4], ensuring sufficiently small steps during the whole simulation.

The cubic mesh of the simulated volume allows for automated adaption within the volumes of interest using a predefined refinement function, which in case of laser material processing focuses on areas of high energy input of the laser as well as phase changes and high temperatures. This refinement and unrefinement facilitates highly accurate calculations while keeping the

computation time at a very low level, compared to calculations using a constant grid.

2.1. Laser-Metal Interaction

In our simulation model, the absorbed and reflected fraction of the laser beam at incidence onto the metal was implemented according to the Fresnel equations. Therefore, a correct estimation of the complex refractive index was necessary.

However, to our knowledge, no experimental data exists for the refractive index of iron or steels in the infrared regime for temperatures around the melting point. So we calculated the complex refractive index both from the Drude model [5], and from the Dausinger model [6] taking interband absorption into account using the electron density [7] and electric conductivity [8] as input parameters. From there, the ratio of angle-dependant absorption and reflection ratio were determined using an approximation of the Fresnel formula [9]. For large wavelengths and high temperatures, the results from both methods agree well.

The energy input of the absorbed beam into the metal was implemented assuming exponential decay inside the metal according to Lambert-Beer, and the reflected beam was modeled using a computation time efficient combination of a ray tracing algorithm and a diffusion based method [10].

Additionally, the absorption in the metal plasma vapor was taken into account since its effect increases drastically with wavelength. Therefore, it was modeled introducing a temperature and density dependent absorption coefficient [11].

2.2. Implemented Physics

The main difficulty in calculating the conductive and convective heat transfer by solving the heat equation in laser material processing is posed by the need of taking the enthalpies during fusion and evaporation, as well as recondensation and resolidification into account.

In our model this problem is approached by using an iterative method based on [12][13], correcting the enthalpies within every calculation step of the heat equation multiple times. Thus, within the first step of each calculation, both enthalpies are neglected. From this first preliminary temperature solution, the enthalpies can be estimated more correctly. These improved values are then used in the subsequent step.

The fluid dynamic within the simulations is modeled incompressibly and is based on mass conservation, the Navier-Stokes equation and the phase transport equation [14]. It is solved using the PISO (Pressure Implicit with Splitting of Operators) algorithm [15].

The description of the evaporation process and the vapor dynamic are predicated on the calculation of the mass of the evaporated material as well as on its associated vapor pressure.

In fusion cutting, the use of the inert process gas is crucial. Due to the difficulties of its implementation, the gas jet is modeled making use of a simplified approach. That means that the gas flow is provided as a constant pressure field defined in the simulated volume above the metal surface rather than modeling the nozzle.

2.3. Simulation Parameters

Collecting accurate material parameters for steel at temperatures around and above the melting point, however, posed a problem that, unfortunately, remains yet unsolved. Therefore, the properties of iron were used, since for this material a consistent and complete set of material parameters around melting temperature could be found in [8,9]. The values are given in Table 1, the thickness of the simulated sheet can be varied arbitrarily, for this paper a value of 1 mm was chosen.

Table 1. Properties of iron at its melting temperature

Physical property	Symbol	Value
Molar mass	M	55.845 g/mol
Density	ρ	7015 kg/m ³
Specific heat	c_p	841.17 J/kgK
Thermal conductivity	λ_T	34.5 W/Km
Viscosity	ν	0.784 m ² /s
Temperature of fusion	T_M	1809 K
Evaporation temperature	T_V	3133 K
Enthalpy of fusion	H_M	272.4 kJ/kg
Enthalpy of evaporation	H_V	6095 kJ/kg
Surface tension	σ	1.872 N/m
Complex refractive index at $\lambda=10.6 \mu\text{m}$	$n+ik$	14,7 + i 15,5

As inert process gas nitrogen was employed. Its thermophysical properties can be found in [16-18].

The parameters of the Gaussian CO₂ laser beam which was defined in the simulation model for this work are given in Table 2.

Table 2. Parameters of the simulated laser

Physical property	Symbol	Value
Wavelength	λ	10.6 μm
Laser power	P_L	4 kW
Beam profile		Gaussian
Waist radius	w_0	100 μm
Feed rate	v_0	0.4 m/s

3. Simulation results and discussion

In Fig. 1, a cross section through the metal sheet along the cutting direction is given for different time steps of the cutting process. The laser beam was orthogonal to the sheet irradiating the metal sheet from the top.

In the beginning of the cutting process, the laser hits the metal sheet and melts and evaporates the material [Fig. 1 (a)]. Then, droplet formation and melt spilling can be observed. Before full penetration of the sheet, the melt is expelled to the top [Fig. 1(b)]. Afterwards, due to the pressure of the process gas, the melt is expelled downwards [Fig. 1 (c-f)].

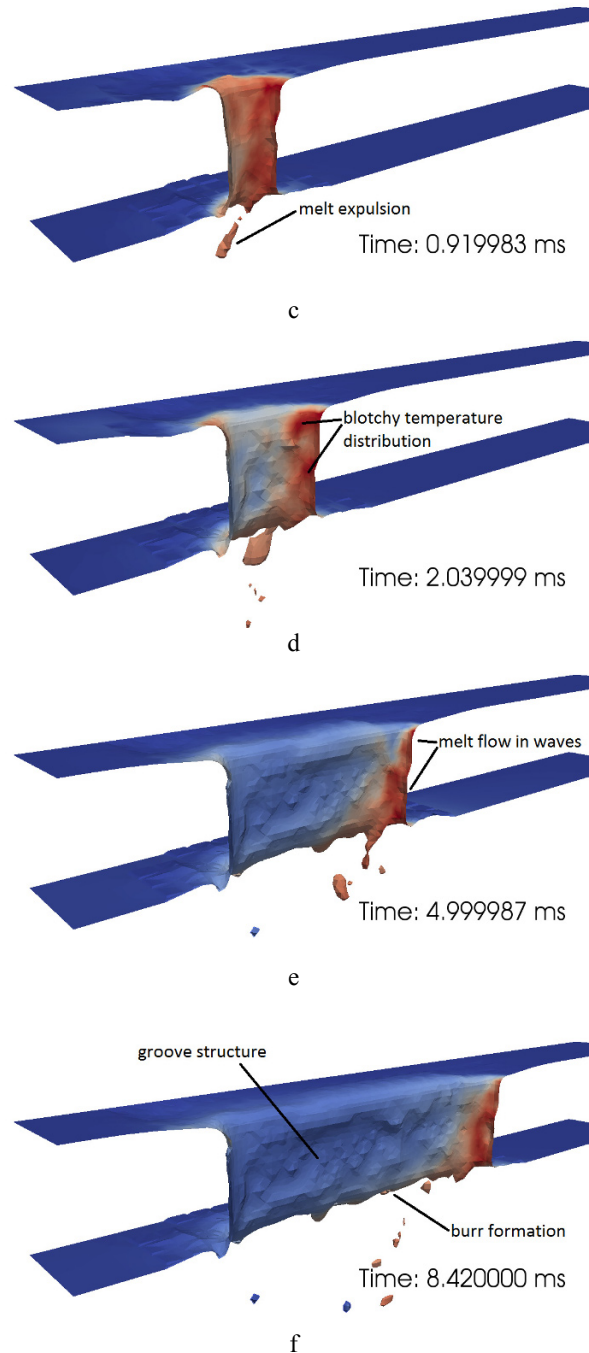
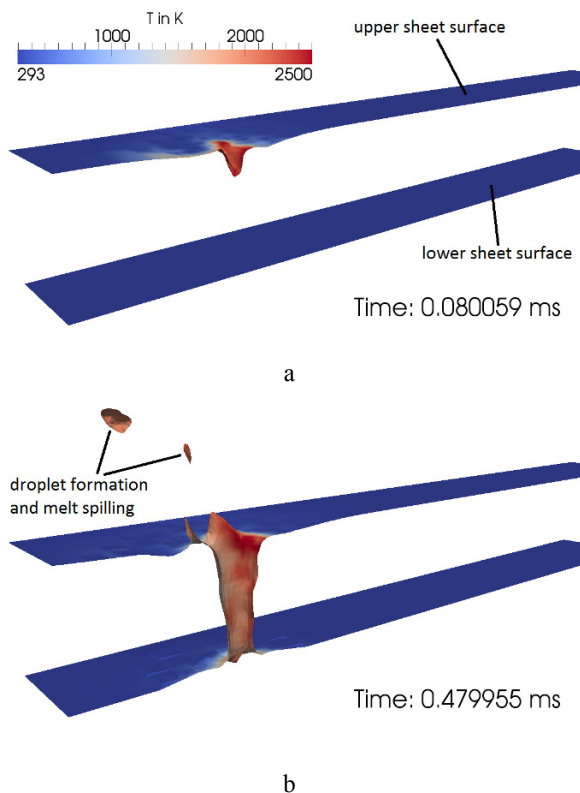


Fig. 1. Simulated laser cutting process using the given model and parameters. The illustrated surface displays the metal-air boundary and the color indicates its temperature. The different panels represent the different time steps (a-f). The color legend is identical for all panels and therefore is given only in panel a

The simulation clearly shows that the melt does not flow away from the cutting front uniformly, but rather in a wavelike process, which can be derived from the curvy cutting front and from its blotchy temperature distribution [Fig. 1 (d-f)].

After cool down of the cutted material, a realistic, rough groove structure along the cutting edge can be observed [Fig. 1 (f)]. Moreover, burr at the lower side of the cutting edge is formed [Fig. 1 (f)].

Figure 2 shows a close-up of the cutting front. For reasons of clarity, the default smoothing interpolation of the temperature field was skipped. Again, a wave within the melt flow can be observed. This wave exhibits a pronounced shadowing effect on the area underneath it, which, hence, cannot be irradiated by the laser and stays considerably cooler. Therefore, the resulting temperature distribution along the cutting front is blotchy.

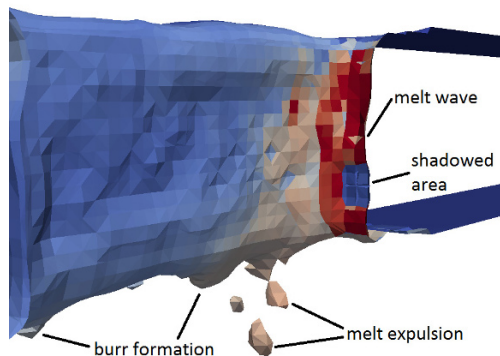


Fig. 2. Close-up of the metal-air boundary of the same cutting simulation. Here, the smoothing of the temperature field was omitted. The melt wave in the middle of the cutting front shadows the area beneath it, which stays significantly cooler

4. Conclusion and Perspectives

In this work, the numerical simulation of the CO₂ based laser cutting process of metal sheets within the framework of OpenFOAM® could be demonstrated. The implemented laser-metal interaction and the physical description of the dynamics proved to be an effective way for the description of this process. The melt flow and expulsion as well as the cutting edge structures showed realistic results.

Acknowledgements: The authors gratefully acknowledge the funding of the project “Thermomechanical and Fluiddynamic Interactions in Laser Deep Penetration Welding” as well as the funding of the Erlangen Graduate School in Advanced Optical Technologies (SAOT) by the German National Science Foundation (DFG) in the frame work of the excellence initiative.

References

- [1] Geiger M, Leitz KH, Koch H, Otto A, (2009) A 3D Transient Model of Keyhole and Melt Pool Dynamics in Laser Beam Welding Applied to the Joining of Zinc Coated Sheets. *Prod. Eng. Res. Devel.* 3:127-136
- [2] Otto A, Koch H, Leitz KH, Schmidt M, (2011) Numerical Simulations – A Versatile Approach for Better Understanding Dynamics in Laser Material Processing. *Phys. Proc.* 12:11-20
- [3] Leitz KH, Koch H, Otto A, Schmidt M, (2012) Numerical Simulation of Process Dynamics During Laser Beam Drilling With Short Pulses. *Appl. Phys. A.* 106:885-891
- [4] Hirt CW, Nichols BD, (1981) Volume of Fluid (VOF) Method for the Dynamics of Free Boundaries. *J. of Comp. Phys.* 39:201-225
- [5] Courant R, Friedrichs K, Lewy H, (1928) Über die partiellen Differenzgleichungen der mathematischen Physik. *Math. Ann.* 100:32-74
- [6] Wooten F, (1972) *Optical Properties of Solids.* London: Academic Press
- [7] Dausinger F, Shen J, (1993) Energy Coupling Efficiency in Laser Surface Treatment. *ISIJ Int.* 33:925-933
- [8] Haynes WM, Lide DR, (2011) *CRC Handbook of Chemistry and Physics.*[e-book] 91st ed. Internet Version 2011. Available through: < <http://www.hbcnetbase.com>> [Accessed 20 June 2011]
- [9] Brandes EA, Brook GB, (1992) *Smithells Metals Reference Book.* 7th ed. Oxford: Butterworth Heinemann
- [10] Prokhorov AM, Konov VI, Ursu I, Mihailescu IN, (1990) *Laser Heating of Metals.* Bristol: IOP Publishing Ltd
- [11] Poprawe R, (2005) *Lasertechnik für die Fertigung.* Berlin: Springer
- [12] Voller VR, Cross M, Markatos NC, (1987) An Enthalpy Method for Convection/Diffusion Phase Change. *Int. J. for Num. Meth. In Eng.* 24:271-284
- [13] Brent AD, Voller VR, Reid KJ, (1988) Enthalpy-Porosity Technique for Modeling Convection-Diffusion Phase Change: Application to the Melting of a Pure Metal. *Num. Heat Trans.* 13:297-318
- [14] Kunkelmann C, Stephan P, (2009) CFD Simulation of Boiling Flows Using the Volume-of-Fluid Method Within OpenFOAM. *Num. Heat Trans.* 56:631-646
- [15] Issa RI, (1985) Solution of the Implicitly Discretised Fluid Flow Equations by Operator-Splitting. *J. of Comp. Phys.* 62:40-65
- [16] Kadoya K, Matsunaga N, Nagashima A, (1985) Viscosity and Thermal Conductivity of Dry Air in the Gaseous Phase. *J. Phys. Chem. Ref. Data.* 14:947-970
- [17] Hanley HJM, Ely JF, (1973) The Viscosity and Thermal Conductivity of Dilute Nitrogen and Oxygen. *J. Phys. Chem. Ref. Data.* 2:735-755
- [18] Span R, Lemmon EW, Jacobsen RT, Wagner W, (1998) A Reference Quality Equation of State for Nitrogen. *Int. J. of Thermodyn.* 19:1121-1132.

Numerical methods for laser path calculation for surface treatment of dies and moulds

Y. Liu, R. Ur-Rehman, D. Heinen and L. Glasmacher
Fraunhofer IPT, Steinbachstrasse 17, 52074 Aachen Germany

Abstract. Utilization of laser based processes such as alloying/dispersing are in frequent use to improve the properties of contact surfaces and consequently to increase the lifetime of moulds and dies. The process involves transmission of energy from laser beam and/or alloying materials in precise amounts and accurately at the desired positions on the part surface. The complexity in the implementation of the processes has been investigated at Fraunhofer IPT and a Computer Aided Manufacturing (CAM) solution has been established to optimize the application of powder based laser processes for surface treatment of moulds and dies. In early part of the paper the background of laser processes for surface treatment technology is discussed, based upon physics knowledge and experiment results. Accordingly, the larger part of the research focused on the analysis and optimization of the CAM strategies and specialization of CNC data for laser machine. The optimization of CAM strategies is achieved by application of numerical methods such as statistic calculation of triangulation and surface parameterization and approximation. A consistent workflow that integrates process database, laser machine simulation and specialized post-processing is employed to achieve stable CAM solution. The results from implementation of CAM solution are also demonstrated.

Keywords: laser surface treatment, CAM solution, CNC, moulds and dies, triangulation mesh, laser path generation

1. Introduction

The manufacture industry is facing constantly the challenge to reduce production costs and increase production volumes at persistent product quality. Being the most common-used tooling in most of the sectors of manufacture industry, moulds and dies are the determinative part influencing the production cost and the part quality. Industrial reports show that increasing forging dies lifetime by 100-200% can reduce the overall costs by 30% [1].

The deterioration of moulds and dies is caused by thermal and mechanical stresses and chemical exposures during their usage. All of these factors result in a high abrasive and adhesive wear of the parts, cracks on the contact surfaces and dimension deviation, which are the

main criteria for useful lifetime of moulds and dies [2] and [3].

The earlier works in [4-7] investigated into the effect of laser process to metallic parts. According to Ayers and Tucker [4] and Tassin [5], laser imparts hard particles into metals and alloys to adjust the dissolution of these particles in the melted substrate, leading to desired metallurgical structures and properties with continuity in the chemical and mechanical properties. Therefore laser alloying/dispersing is an effective and economic approach to extend the useful lifetime of dies and moulds by enhancing the mechanical and chemical characteristics of contact surface material. For instance, a combined laser alloying and nitriding treatment process can produce a hard surface layer of 0.5- 1.0 mm case depth and a hardness of up to 1000 HV that ensures wear resistance and fatigue resistance [8]. In addition, the compound treated layer enhances good tribological and corrosion resistance properties of the die surface [6].

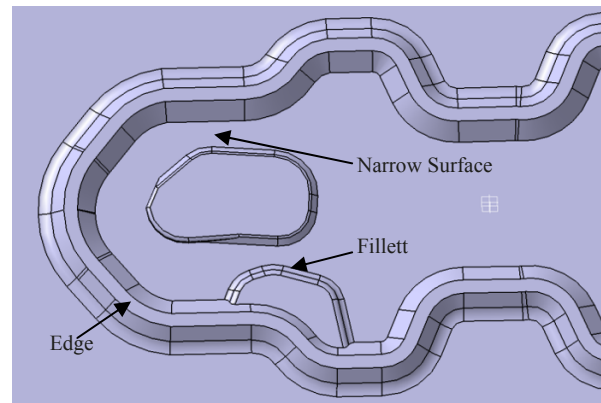


Fig. 1. Typical geometric features on moulds and dies for surface treatment

Although laser processes have advantages that surfaces can be treated with dimensional precision and efficient control of thermal energy, however there are challenges

in the application of these processes on the complex geometries in industrial practice. The critical areas of moulds and dies are typically narrow and small geometric features, e.g.: which are shown in Fig. 1 of a die for forming processes. These areas normally consist of freeform surface, and surrounded by wall structure that leads to collision risk to the laser head. The investigations at Fraunhofer IPT have considered these problems during laser surface treatment and utilized 5-axis CNC laser machine to accomplish the application on all critical areas and to ensure the precision of the laser process [12].

To improve the efficiency of the surface treatment process chain, an automatic planning of laser path through computer aided manufacturing (CAM) has been strongly realized and CAM solution has been established at Fraunhofer IPT to achieve the process requirements in an integrative method. The CNC machines are programmed with NC data that is a combination of laser path and technological parameters for laser surface treatment. The NC programming is automatically accomplished by an integrated CAM solution to control the risk of process failure and to reduce the overall cost of prototypes for destructive testing as well as regular production.

2. Knowledge of laser alloying/dispersing process

The understanding of the physics of laser processes is essential for the development of an efficient surface treatment process to enhance the properties of part material. The laser beam heats up the local areas near the die's surface and melts them. Meanwhile powdered materials (e.g WC-Co-Cr, TiC or VC) are conveyed into the melting pool through an inert gas stream and completely diffuse into solution. The Fig. 2 below presents a schematic representation of the processes [12]. In typical applications the process utilizes a Nd:YAG or diode laser source that can concentrate 1.0~2.0 kws in a spot diameter/size of 0.8~2.0 mm.

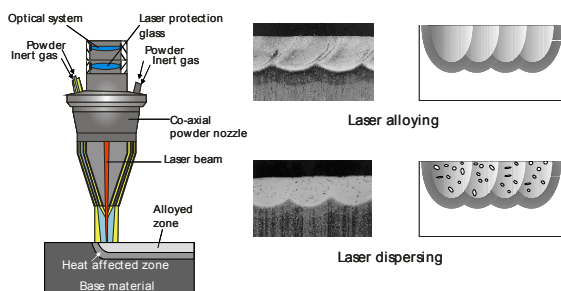


Fig. 2. Schematic arrangement of laser surface treatment process

Fraunhofer IPT carried out experimental investigation in the scope of European Commission's funded research project CURARE to achieve optimal surface treatment process and to identify the criteria for the stability of process. During these experiments the physics of

interactions between laser and the material has been investigated [12].

The experimental setup consisted of machine + laser has been built up to investigate into the effects of laser intensity, alloying materials and their amounts, gas flow upon the surface and the formation of heat effected zones. Fig. 3. shows the influence of the process on the surface and below the surface. The performance of the following milling and grinding processes has also been verified on the test parts. The laser process is carried out by a computer numerical controlled (CNC) machine - Alzmetall GS-1005 LOB, integrated with a Precitec laser head.

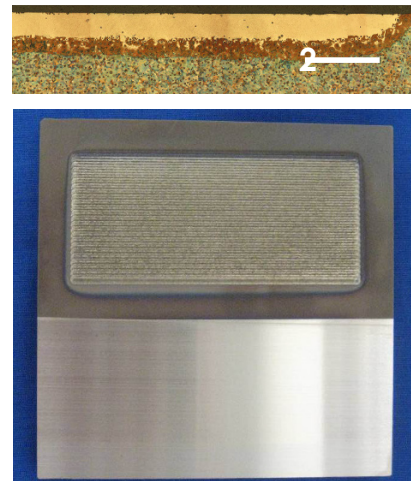


Fig. 3. Cross section of alloyed cast part, its alloyed surface and milled/grinded surface

3. CAM solution for planning for laser process

The control of surface treatment process is complex since it involves the control of simultaneous movements of laser in five degrees of freedom (5-axis CNC). The objective of CAM solution for laser process is to automatically generate precise laser path together with consideration of laser technological requirements, NC machine specialty and characteristics of geometry features on moulds and dies.

The CAM module developed at Fraunhofer IPT for laser process for surface treatment uses given geometry features on part as input for laser path calculation. The CAM solution automatically generates interpolated move positions on part surface within allowable tolerance and outputs the NC data for laser process for surface treatment. Based upon the types of data structure of input geometry, CAM strategies can be categorized into two groups: parametric surface-based and triangulated mesh-based. The specialized requirements for laser surface treatments have been investigated and handled by representing the part geometry by a triangulated mesh and integrating laser processes into advanced numerical

techniques for calculation of laser path for modern CNC laser machine.

3.1. Surface-based laser path calculation

Surface-based calculation is aiming at CAD data consisting of NURBS surfaces/curves. This type of data is normally input as IGES or STEP file, and then a 3D model is built up as an intermediate of interpolation [11].

The first step is to build-up a data structure with 2-dimensional (u-v) parameterized surface model from CAD data. The u-v net combined with correspondent to the 3D coordinates positions are generated from the NURBS geometries. The procedure of laser path generation can be described as following steps:

1. Parameterize surfaces and boundary curves from 3D space into u-v space
2. Based on types of CAM strategy and laser setup, build up virtual intersection of part surface and laser
3. Calculate intersection points (moves) between the intersection geometries and parameterized surface on laser path, as in Fig. 4
4. Refine the laser path by interpolating positions between intersections within specified tolerance
5. Re-group the points and store into data structure for laser path according to CAM strategy configuration
6. Calculate orientation of laser at each position in the laser path, based upon the user's configuration of laser process and to avoid collision of laser head with die/mould and accordingly re-adjust move position when necessary

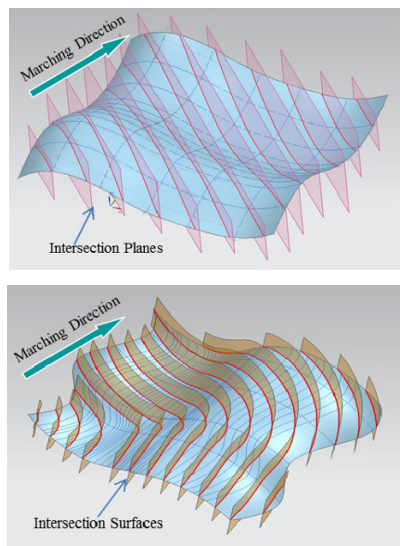


Fig. 4. (a). calculation of iso-planer laser path (b). calculation of constant offset laser path

The Fig 4 shows two typically used strategies. (a) illustrates the interpolation geometries used in the strategy “Iso-planer Parallel moving”, and 4 (b) demonstrates the strategy “Constant offset morphing from

curves”, which means laser path offsets from the initial curve.

3.2. Triangulated mesh-laser path calculation

In some application cases, only a triangulated-mesh is given as the input geometry for laser path calculation, for example data acquired from laser metrology process. The difficulty in such applications is that we cannot directly obtain continuous and analytic information within the triangulated mesh, but only discrete data of part surface such as vertices and edges.

We propose a set of mesh-based laser path calculation methods to solve this problem. The procedure can be divided into two steps:

1. Generation of initial geometries
2. Propagation of laser path based on initial geometries

Firstly we build up an extended “graph” data structure which stores the 3D dimension information of the mesh, such as vertices, edges and faces, and also the topologic information such as query of neighbour facets. Then statistic and topologic methods are used to obtain these features from the graph, also combined with empirical knowledge of part geometry, such as estimation of the tensor of the local curvature, triangle normal voting method to detect edges and intersection between analytic geometry elements and triangulated mesh.

Afterwards a rapid algorithm generates the laser path as propagating curves from the initial geometries. A “map” structure that represents the geodesic distances from vertices to initial geometry is established on the mesh edges or vertices, by an optimized algorithm based on Fast Marching Method (FMM) [9, 10]. This method spreads the laser path on the mesh in a similar pattern as wave-front propagation, with time complexity by $O(n \log(n))$, in which n is the number of vertices. The picture below demonstrates an example of mesh-based laser path generated by our method.

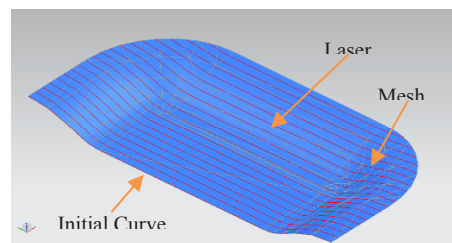


Fig. 5. Laser path generated on mesh

4. Simulation and prototype test result

A post-processor is implemented to translate the calculated laser path to NC program specialized for the laser machine. We preceded an analysis of the time-sequence and the interactions among system components

including laser controller, inert gas pump, powder conveyor and machine kinematics.

A machine simulation module developed based on ModuleWorks simulation libraries [13] has been integrated into the CAM system and applied to check collision of machine kinematic components and work piece, before the generated 5-axis NC program runs on the laser machine. The following picture illustrates an example of a demonstrator for alloying testing.

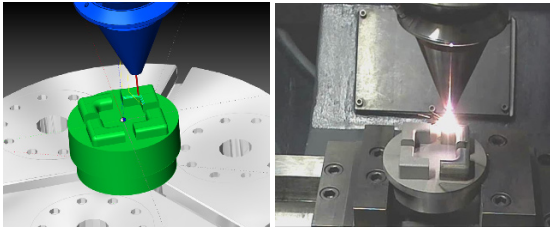


Fig. 6. Simulation and real process

A testing part is made of steel 1.2379. The powder used for alloying is WC-Co-Cr. The alloyed result is shown in the picture below:

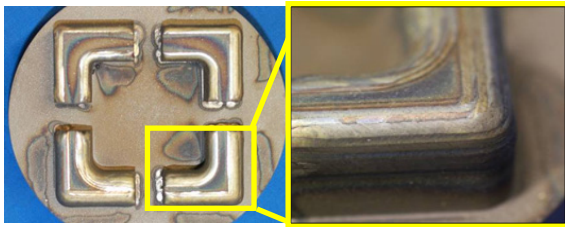


Fig. 7. Test result

A metallographic inspection has been made and showed that with proper process parameter setting, the alloyed depth on processed area can reach up to 1.5 mm and the hardness reaches to 800 HV0.3.

5. Conclusion

In this paper we introduced two sets of numerical methods for laser path calculation, respectively for parametric surface model and triangulated-mesh geometry. These methods have been integrated into a CAM system, together with a specialized post-processor to generate NC data for laser CNC machine. The CAM systems integrate a machine simulation to check the NC data and prevent any unforeseen collision of machine components. Tested parts show that the surface quality on the treated areas has been significantly improved. The CAM systems have also been utilized in several industrial applications and have demonstrated to be effective and efficient to improve the useful life of the dies and moulds.

Acknowledgement: The authors would like to express their gratitude to European Commission for supporting CURARE project (grant number 222317) of seventh Framework Program. The cooperation and support of CURARE consortium partners is highly appreciated.

Reference

- [1] Hejarsmide NN, (01/2002) Forging Company Hejarsmide, Sweden. www.hejarsmide.se
- [2] Robert F, (2008) Standzeitverlängerung von Werkzeugen durch Laserbehandlung und Nitrieren. *Giesserei* 95 H. 5:110–111
- [3] Harksen S, Glaeser T, Bleck W, Klocke F, (06/2009) Beurteilung von Temperaturwechsel und Mechanischem Verschleiß auf duplexbehandeltem Warmarbeitsstahl. Proceedings of the 8th International Tooling Conference, 8ITC, Mainz
- [4] Ayers JD, Tucker TR, (1980) Particulate-TiC-Hardened steel surfaces by laser melt injection. *Thin Solid Film* 73-1:201-207
- [5] Tassin C, Laroudie F, Pons M, Lelait L, (03/1996) Improvement of the wear resistance of 316L stainless steel by laser surface alloying. *Surface and Coatings Technology* 80/1–2:207-210
- [6] Gläeser T, (2006) Standzeitverlängerung von Werkzeugen und Formen durch Laserlegieren/-dispergieren und Nitrieren, VDFW im Dialog. *Magazin des Verbands Deutscher Werkzeug- und Formenbauer e. V.*, Ausgabe 03
- [7] Gläeser T, (2006) Standzeiterhöhung von Schmiede- und Druckgießwerkzeugen durch Laserlegieren/-dispergieren und Nitrieren. *Laser Magazin*, Ausgabe 03
- [8] Ruset C, Grigore E, Gläser T, Bausch S, (2006) Combined treatments – a way to improve surface performances. The fifth International Edition of Romanian Conference on Advanced Materials, Bucharest-Magurele, Romania, Sept. 11-14, 2006
- [9] Sethian JA, (02/1996) A Fast Marching Level Set Method for Monotonically Advancing Fronts, *PNAS (Proceedings of the National Academy of Sciences of the United States of America)*, Vol. 93-4:1591-1595
- [10] Kimmel R, Sethian JA, (07/1998) Computing geodesic paths on manifolds. *PNAS (Proceedings of the National Academy of Sciences of the United States of America)* vol. 95:8431-8435
- [11] Ur-Rehman R, (07/2010) Numerical Techniques for CAM Strategies for Machining of Mould and Die, Proceedings of the 36th International Matador Conference 6: 259-262
- [12] Klocke F, Heinen D, Ruset C, Liu Y, Arntz K, (2010) Kombinierte Oberflächenbehandlung von Werkzeugen, *wt Werkstattstechnik online Jahrgang* 100
- [13] ModuleWorks CNC simulation and toolpath verification CAD/CAM components, <http://www.moduleworks.com/cad-cam-components/simulation-verification.asp>, ModuleWorks GmbH